Dynamical Systems
Vol. 00, No. 00, February 2009, 1–15

RESEARCH ARTICLE

Delay Induced Canards in High Speed Machining

Sue Ann Campbell
Department of Applied Mathematics
University of Waterloo
Waterloo, Ontario, N2L 3G1 Canada
and
Emily Stone
Department of Mathematical Sciences
The University of Montana
Missoula, MT 59812 U.S.A.
and
Thomas Erneux
Université Libre de Bruxelles
Optique Nonlinéaire Théorique
Campus Plaine, C.P. 231, 1050 Bruxelles
Belgium
(*September 4, 2009*)

We consider here a model from [1] for regenerative chatter in a drilling process. The model is a nonlinear delay differential equation where the delay arises from the fact that the cutting tool passes over the metal surface repeatedly. For any fixed value of the delay, a large enough increase in the width of the chip being cut results in a Hopf bifurcation from the steady state, which is the origin of the chatter vibration. We show that for zero delay the Hopf bifurcation is degenerate and that for small delay this leads to a canard explosion. That is, as the chip width is increased beyond the Hopf bifurcation value, there is a rapid transition from a small amplitude limit cycle to a large relaxation cycle. Our analysis relies on perturbation techniques and a small delay approximation of the DDE model due to Chicone [2]. We use numerical simulations and numerical continuation to support and verify our analysis.

1. Introduction

In this paper we document the occurrence of canards in a constant delay system developed for modeling metal cutting processes such as drilling. Canards were first studied by a group of French mathematicians (E. Benoît, J.-L. Callot, F. Diener, and M. Diener) in the context of relaxation oscillations of the Van der Pol equation with a constant forcing term ([3], [4]). Close to a Hopf bifurcation in this system, a small change of the control parameter leads to a fast transition from a small amplitude limit cycle to a large amplitude relaxation cycle. The fast transition is called canard explosion and happens within an exponentially small range of the control parameter. Because this phenomenon is hard to detect it was nicknamed a canard, after the French newspaper slang word for hoax. Furthermore, the shape of the limit cycle immediately following the transition has a knob-like corner reminiscent of a duck's beak. So the notion of a canard cycle/explosion was born and the chase after these creatures began following either nonstandard ([4]) or standard ([5]) methods.

The discovery of the canard cycles by the end of the seventies was aided by new

ISSN: 1468-9367 print/ISSN 1468-9375 online

DOI: 10.1080/14689360xxxxxxxxxxxxx
http://www.informaworld.com

computational methods for the systematic simulation of bifurcation of solutions in the phase plane. Over the past decade, there has been increased interest in delay differential equations (DDEs). Previously studied equations have been re-investigated allowing for a better physical understanding of old problems, and new areas of research have appeared. Of particular interest are dynamical phenomena that are directly generated by the delayed variable. These include, for example, the stabilization of unstable steady states [6], the emergence of square-wave oscillations for first order DDEs [7], or the secondary bifurcation to quasi-periodic oscillations for second order DDEs [8]. In this paper, we concentrate on a mechanical model for high-speed drilling and investigate the limit of small delays. This limit is singular and we construct and analyze the emergence of strongly pulsating oscillations by both numerical and asymptotic techniques.

The plan of the paper is as follows. In Section 2, we formulate the evolution equation for the machine-tool system subject to a delayed feedback. In Section 3, we investigate the small delay limit corresponding to the high speed revolution of the spindle of the cutting machine. We note that the equation of motion for zero delay can be reformulated as a weakly perturbed conservative problem and anticipate a non-trivial effect of the delayed feedback. In Section 4, we construct the limit-cycle solution that emerges from the Hopf bifurcation using an averaging technique appropriate for weakly perturbed but strongly nonlinear conservative oscillators. We determine the critical value of the control parameter where the amplitude of the oscillations suddenly increase (canard explosion). The validity of our asymptotic analysis is then evaluated in Section 5 by systematic comparisons between the numerical bifurcation diagram of the original DDE, its ODE approximation for small delay, and the analytical predictions. Finally, we discuss in Section 6 the impact of our results for the original mechanical system and, more generally, DDEs that exhibit similar bifurcation properties. In particular, we explain how dramatic changes of the amplitude and waveform of the oscillations are possible near a Hopf bifurcation even if the delay is small.

2. Chatter in Machining Models

In a previous paper one of us [1] documented the development of a model for a certain type of regenerative chatter in drilling processes. This model incorporated nonlinear friction on the tool face interacting with fundamental axial-torsional vibrations found in some twist drills. Metal cutting processes such as turning, milling and drilling, are plagued with an instability to self-sustained vibrations that can ruin both the tool and the work piece, due to the fact that the tool cuts over a surface repeatedly at a constant frequency. This phenomenon is called regenerative chatter, and is modeled by fixed delay differential equations, since the force on the cutting tool depends on the thickness of chip being removed, and this depends on the position of the tool one revolution prior to the current position.

In engineering applications an operation such as metal cutting is modeled by considering distinct vibrational modes of the apparatus and their interaction with external forces. See figure 1. The vibrations are assumed to be linear, with large inertia and stiffness, and small damping. Thus the equation of motion of a machine tool vibration mode excited by a cutting force is

$$\ddot{x} + c\dot{x} + \omega_0 x = F(x, \dot{x})$$

where $x(t)$ is the amplitude of the vibration, c is the effective damping, and ω_0 is the natural frequency of the mode. The forcing function, $F(x, \dot{x})$, is the projection

of the cutting force onto the vibration direction, which occurs at an angle θ with respect to the vertical from the tool path. The cutting force has the general form

$$F(x, \dot{x}) = F((x(t) - x(t-\tau)), \dot{x}(t)),$$

where τ is the period of revolution of the spindle of the cutting machine. This means it is proportional to the chip thickness (i.e., $(x(t) - x(t-\tau)$, the difference between the position at the time t, and the time one revolution ago), and the penetration rate $\dot{x}(t)$. Thus τ is the delay parameter in the delay differential equation.

The specific form of the cutting force was determined from the Merchant-Oxley model of steady orthogonal cutting ([9], [10]) and is

$$F(x, \dot{x}) = wT(t_1 - (x - x(t-\tau))\cos\theta)(p_0 + p_1\dot{x} + p_2\dot{x}^2). \tag{1}$$

It depends on the instantaneous chip thickness, given by the expression $(t_1 - (x(t) - x(t-\tau))\cos\theta)$, where t_1 is the nominal chip thickness set by the machine feed. The polynomial in $\dot{x}$ is a truncation of an asymptotic expansion for a nonlinear stick-slip type friction force. The expansion coefficients p_0, p_1, and p_2, depend on cutting speed, rake angle of the tool, and vibration angle. For the conditions considered in [1] both p_1 and p_2 are quite small for all vibration angles, two to four orders of magnitude smaller than p_0 in most cases. The other parameters are w, the chip width, and T, the strength of the material. In [1] these parameters were set at values typical for machining aluminum, namely $w = 6.35 \times 10^{-3}m$, $T = 276$ MPa, $t_1 = 7.6 \times 10^{-5}m$.

Two modes of vibration were considered in our earlier work. A traditional milling mode where the vibration occurs perpendicular to the workpiece, and an axial-torsional mode where vibrations occur across the first and third quadrants, corresponding to a motion where the drill lengthens when it "unwinds". A three dimensional vibration analysis revealed that this vibration angle is (approximately) $\theta = 1.38 = 79°$. In this case both p_0 and p_1 are less than zero. For a vertical vibration θ is zero, and p_0 and p_1 are positive for the rake angles of the tool that we considered.

After a non-dimensionalization we arrive at the following equation of motion for the new amplitude variable, η,

$$\eta'' + \gamma\eta' + \eta - \beta\left[1 - (\eta - \eta(t-\tau))\cos(\theta)\right](p_0 + \bar{p}_1\eta' + \bar{p}_2\eta'^2) = 0. \tag{2}$$

In this equation, prime means differentiation with respect to the dimensionless time $\bar{t} \equiv \omega_0 t$, where ω_0 is the vibrational frequency of the mode. The dimensionless amplitude η is the vibration amplitude normalized by the nominal chip thickness t_1. Our objective here is to investigate the limit of small delays (small τ), that is, the high-speed cutting limit. As we shall demonstrate, this limit is singular and requires careful study. In what follows we drop the bar on the rescaled t variable.

Introducing the deviation from the steady state, $y \equiv \eta - \beta p_0$, eq. (2) can be rewritten as

$$\begin{aligned} y'' + \gamma y' + y = {} & \beta(\bar{p}_1 y' + \bar{p}_2 y'^2) - \beta p_0\cos(\theta)(y - y(t-\tau)) \\ & -\beta\bar{p}_1\cos(\theta)y'(y - y(t-\tau)) \\ & -\beta\bar{p}_2\cos(\theta)y'^2(y - y(t-\tau)). \end{aligned} \tag{3}$$

This is the form of the model we will study in this paper. We will refer to it as the **DDE model**.

From the linearization of this equation, we can determine the characteristic equation for the growth rate, and from this the conditions for a purely imaginary eigenvalue. To do so we substitute $z = e^{i\omega t}$ (the neutrally stable solution) into the equation (3) and set the coefficients of the real and imaginary parts equal to zero. These two equations can be solved for β and τ as a functions of ω, namely

$$\tau(\omega) = \frac{2}{\omega}(\arctan(\frac{1-\omega^2}{\Gamma\omega}) + n\pi), \quad \beta(\omega) = \frac{1}{2p_0\cos\theta}\{\frac{(\Gamma\omega)^2}{\omega^2-1} + (\omega^2-1)\}. \quad (4)$$

We have set $\Gamma = \gamma - \beta p_1$, and assume that $\Gamma > 0$, to guarantee stability in the unforced case. Note that $n = 0, 1, 2, \ldots$ determines the branch of the arctangent function. For fixed values of the physical parameters, (4) yields the parametric equations, $\tau = \tau(\omega)$, $\beta = \beta(\omega)$, describing curves in the β, τ parameter space. The $n = 0$ branch is plotted in Figure 2, which ranges over small values of τ.

In [11] we compute the Hopf stability coefficient along this boundary via a center manifold approximation [12–14]. In the case of the traditional vibration mode the Hopf bifurcation is supercritical for values of τ below 0.5. In this study we will limit ourselves to this case and to small τ values, so the Hopf bifurcation will always be supercritical in what follows.

As observed in [11], the system exhibits interesting behaviour for small values of τ. In particular, as β is increased from the bifurcation value, there is a rapid transition from small amplitude to large amplitude limit cycles. It is the purpose of this paper to show that this transition is caused by a canard explosion. In particular, we shall show that the canard transition is induced by perturbing in the delay term from a singular limit.

3. The High Speed/Small Delay Limit ($\tau \to 0$)

We begin by considering the case $\tau = 0$. In this situation, eq. (3) reduces to

$$y'' + (\gamma - \beta\bar{p}_1)y' + y = \beta\bar{p}_2 y'^2. \quad (5)$$

The characteristic equation of the linearization of (5) about the trivial solution has a pair of pure imaginary eigenvalues, $\pm i$, if $\beta = \gamma/\bar{p}_1 \stackrel{def}{=} \beta_0$. It was noted in [11] that the Hopf bifurcation in this model is degenerate, since the cubic coefficient of the normal form is zero. In fact, more can be said.

Consider eq. (5) with $\beta = \beta_0$

$$y'' + y - \beta_0\bar{p}_2 y'^2 = 0. \quad (6)$$

It is easily shown that this equation is conservative with a one parameter family of solutions given by

$$e^{-2\beta_0\bar{p}_2 y}\left(y'^2 - \frac{1}{\beta_0\bar{p}_2}\left(y + \frac{1}{2\beta_0\bar{p}_2}\right)\right) = C.$$

Now $C = -\frac{1}{2\beta_0^2\bar{p}_2^2} = C_{min}$ corresponds to the equilibrium point at the origin, while $C_{min} < C < 0$ corresponds to periodic orbits surrounding this equilibrium point. For $C > 0$ the solutions are unbounded. The separatrix between the two solution

types is given by the invariant curve defined by $C = 0$, which is

$$y = \beta_0 \bar{p}_2 y'^2 - \frac{1}{2\beta_0 \bar{p}_2}. \tag{7}$$

Some representative solution curves are shown in bold in Figure 3. Other equivalent forms of eq. (6) and its first integral are possible see [15, 16].

For τ sufficiently small it can be shown, using the results of Chicone [2], that the DDE model (3) has a two dimensional inertial manifold. Restricted to this manifold, the term $y(t) - y(t-\tau)$ in the vector field is approximated by $\tau y'(t)$. That is, the long term behaviour of solutions of (3) is well approximated by the behaviour of the solutions of the following ordinary differential equation

$$y'' + (\gamma - \beta\bar{p}_1)y' + y = \beta\bar{p}_2 y'^2 + \tau\left[-\beta\cos(\theta)(p_0 y' + \bar{p}_1 y'^2 + \bar{p}_2 y'^3)\right]. \tag{8}$$

This equation is central to the analysis of the rest of the paper and will be referred to as the **inertial manifold ODE**. In particular, we investigate eq. (8) in the limit of small τ and compare our asymptotic approximation with the numerical solution of the DDE model (3) in Section 4.

We begin with some basic results. Standard calculations [17] show that (8) has a supercritical Hopf bifurcation of the trivial solution at $\beta = \gamma/(\bar{p}_1 - \tau p_0\cos(\theta)) = \beta_H$. Since τ is close to zero, we may write

$$\beta_H = \frac{\gamma}{\bar{p}_1} + \frac{\gamma p_0\cos(\theta)}{\bar{p}_1^2}\tau + O(\tau^2). \tag{9}$$

This shows how the bifurcation parameter β_H depends on the small parameter τ. More terms in the expansion can be obtained by returning to the characteristic equation of the DDE model (3) and expanding β and ω in τ. In this case one finds

$$\beta_H = \frac{\gamma}{\bar{p}_1}\left[1 + \frac{p_0}{\bar{p}_1}\cos(\theta)\tau + O(\tau^2)\right] \tag{10}$$

$$\omega_H = 1 + \frac{\gamma}{4\bar{p}_1} p_0\cos(\theta)\tau^2 + O(\tau^3), \tag{11}$$

which motivates an asymptotic analysis valid for small τ.

4. Perturbing from the Singular Hopf

The limit $\tau \to 0$ is singular if $\gamma - \beta\bar{p}_1 = O(\tau)$ because eq. (8) reduces to eq. (6), a conservative problem admitting a family of periodic solutions. To determine how these periodic solutions persist for small τ, we must investigate the higher order problem in τ. Assuming

$$\beta = \beta_0 + \tau\beta_1 + .. \tag{12}$$

with $\beta_0 = \frac{\gamma}{\bar{p}_1}$ as previously defined, Eq. (8) simplifies to

$$y'' + y - \beta_0\bar{p}_2 y'^2 = \tau g(y') + O(\tau^2) \tag{13}$$

where

$$g(y') = \beta_1(\bar{p}_1 y' + \bar{p}_2 y'^2) - \beta_0 \cos(\theta)(p_0 y' + \bar{p}_1 y'^2 + \bar{p}_2 y'^3).$$

and β_1 is the bifurcation parameter.

The Hopf bifurcation point now corresponds to $\beta_1 = \beta_{1H}$ where

$$\beta_{1H} = \beta_0 \cos(\theta)\frac{p_0}{\bar{p}_1}. \tag{14}$$

Close to the Hopf bifurcation point, the orbits remain bounded by the separatrix of the conservative system. At a critical value of β_1 the limit-cycle changes dramatically from a small to a large amplitude orbit. We note that the $y' = 0$ nullcline for (13) at the Hopf bifurcation value lies close to the critical manifold that determines the shape of the orbit.

4.1. *Limit cycles from the Hopf bifurcation*

We now determine how the periodic solutions arising from the Hopf bifurcation of eq. (13) depend on the bifurcation parameter β_1. To begin, we rewrite (13) as a system and rescale the variables via $v_1 = \beta_0 \bar{p}_2 y,\ v_2 = \beta_0 \bar{p}_2 y'$ to obtain

$$\begin{aligned} v_1' &= v_2 \\ v_2' &= -v_1 + v_2^2 + \tau G(v_2) + O(\tau^2)\,, \end{aligned} \tag{15}$$

where

$$\begin{aligned} G(v_2) &= (\beta_1 \bar{p}_1 - \beta_0 p_0 \cos(\theta))\, v_2 + \left(\frac{\beta_1}{\beta_0} - \frac{\bar{p}_1}{\bar{p}_2}\cos(\theta)\right) v_2^2 - \frac{\cos(\theta)}{\beta_0 \bar{p}_2} v_2^3 \\ &= G_1 v_2 + G_2 v_2^2 - G_3 v_2^3. \end{aligned}$$

We next seek solutions of (15) of the form

$$\begin{aligned} v_1(t,\tau) &= v_{10}(t) + \tau v_{11}(t) + \cdots \\ v_2(t,\tau) &= v_{20}(t) + \tau v_{21}(t) + \cdots \end{aligned}$$

Substituting this into (15) we find (as expected) that the system for the leading order terms is conservative, with a one parameter family of solutions given by

$$e^{-2v_{10}}\left(v_{20}^2 - v_{10} - \frac{1}{2}\right) = L, \tag{16}$$

where L is a constant. For $-1/2 < L < 0$ the solutions are periodic with period $P(L)$. Setting $L = 0$ gives the separatrix between the periodic solutions and unbounded solutions: $v_{10} = v_{20}^2 - 1/2$.

We wish to find the periodic solutions which persist for $\tau > 0$. To do this we follow the averaging technique of [15, 16]. Consider the variable corresponding to the conserved quantity for the $\tau = 0$ system

$$N(t,\tau) = e^{-2v_1(t,\tau)}\left(v_2(t,\tau)^2 - v_1(t,\tau) - \frac{1}{2}\right). \tag{17}$$

If v_1 and v_2 are $P(L)$ periodic in t, then N will be, too. Thus, a condition for existence of a periodic solution is given by

$$\int_0^{P(L)} \frac{dN}{dt} dt = 0.$$

Using eqs. (15) and (17) the solvability condition to $O(\tau^2)$ becomes

$$0 = \int_0^{P(L)} 2e^{-2v_{10}}(G_1 v_{20}^2 + G_2 v_{20}^3 - G_3 v_{20}^4)\, dt. \tag{18}$$

Noting that $v_{10}(P(L)-t) = v_{10}(t)$ and $v_{20}(P(L)-t) = -v_{20}(t)$ for any $t \in [0, P(L)]$, this further simplifies to

$$0 = \int_0^{P(L)/2} e^{-2v_{10}}(G_1 v_{20}^2 - G_3 v_{20}^4)\, dt.$$

Rewriting this in terms of the original parameters gives

$$(\beta_1 \bar{p}_1 - \beta_0 p_0 \cos(\theta)) \int_0^{P(L)/2} e^{-2v_{10}} v_{20}^2\, dt - \frac{\cos(\theta)}{\beta_0 \bar{p}_2} \int_0^{P(L)/2} e^{-2v_{10}} v_{20}^4\, dt = 0$$

or

$$\beta_1 = \left[\frac{\beta_0\, p_0}{\bar{p}_1} + \frac{1}{\beta_0\, \bar{p}_1\, \bar{p}_2} H(L) \right] \cos(\theta), \tag{19}$$

where

$$H(L) = \frac{\int_0^{P(L)/2} e^{-2v_{10}} v_{20}^4\, dt}{\int_0^{P(L)/2} e^{-2v_{10}} v_{20}^2\, dt} \stackrel{def}{=} \frac{I_1(L)}{I_2(L)}.$$

Using (15) and (16), the integrals may be expressed in terms of v_{10}:

$$I_1(L) = \int_{vl(L)}^{vr(L)} e^{-2v_{10}} (e^{2v_{10}} L + v_{10} + \frac{1}{2})^{3/2}\, dv_{10},$$
$$I_2(L) = \int_{vl(L)}^{vr(L)} e^{-2v_{10}} \sqrt{e^{2v_{10}} L + v_{10} + \frac{1}{2}}\, dv_{10},$$

where $vl < vr$ are the two v_{10} intercepts of the limit cycle, i.e., the roots of $e^{-2v_{10}}(v_{10} + 1/2) + L = 0$. Eq. (19) relates the bifurcation parameter β_1 to L, the constant of the conservative system and hence to the amplitude of the corresponding solution of the unperturbed equation, (v_{10}, v_{20}). For particular parameter values the integrals can be computed numerically. A bifurcation diagram can be obtained in this way and is shown in Figure 4.

To find the critical value of β_1 where the amplitude of the periodic solution becomes unbounded, we take the limit of $H(L)$ in (19) as L approaches 0 (the value corresponding to the separatrix). Let

$$\lim_{L \to 0} H(L) = \lim_{L \to 0} \frac{I_1(L)}{I_2(L)}.$$

Note that the limits of both integrals exist and are given by:

$$I_{10} = \lim_{L\to 0} I_1(L) = \int_{-1/2}^{\infty} e^{-2v_{10}}(v_{10}+\frac{1}{2})^{3/2}\, dv_{10},$$
$$I_{20} = \lim_{L\to 0} I_2(L) \int_{-1/2}^{\infty} e^{-2v_{10}}\sqrt{v_{10}+\frac{1}{2}}\, dv_{10}.$$

Applying integration by parts to I_{10} yields $I_{10} = 3/4 I_{20}$, which gives the critical value of β_1:

$$\beta_1 = \left[\frac{\beta_0\, p_0}{\bar{p}_1} + \frac{3}{4}\frac{1}{\beta_0\,\bar{p}_1\,\bar{p}_2}\right]\cos(\theta) \stackrel{def}{=} \beta_c. \tag{20}$$

4.2. *Trajectories*

In the previous section, we showed that for β_1 close enough to β_{1H} one periodic solution exists for each value of β_1. In addition, numerical simulations such as that in Fig. 6 show that for β_1 large enough the system exhibits large amplitude relaxation oscillations. In this section, we shall show that the limit cycles arising from the Hopf bifurcation connect to the relaxation oscillations at a critical value $\beta_1 = \beta_c$, following the approach of [15].

To begin, we rewrite eq. (13) as first order system:

$$\begin{aligned} y_1' &= y_2 \\ y_2' &= -y_1 + \beta_0\bar{p}_2 y_2^2 + \tau g(y_2). \end{aligned} \tag{21}$$

Recall from eq. (7) that the $\tau = 0$ separatrix is given by

$$y_1 = \beta_0\bar{p}_2 y_2^2 - \frac{1}{2\beta_0\bar{p}_2}.$$

We look for solutions close to this separatrix via an expansion in τ:

$$y_1(y_2) = \beta_0\bar{p}_2 y_2^2 - \frac{1}{2\beta_0\bar{p}_2} + \tau h(y_2) + O(\tau^2)$$

Differentiating this expression with respect to y_2 and using (21) gives the following equation for $h(y_2)$

$$\frac{dh}{dy_2} - 4\beta_0^2\bar{p}_2^2 y_2 h = -4\beta_0^2\bar{p}_2^2 y_2 g(y_2).$$

Solving this ODE with initial condition $h(y_{20}) = h_0$ gives

$$h(y_2) = h_0 e^{2\beta_0^2\bar{p}_2^2(y_2^2-y_{20}^2)} - e^{2\beta_0^2\bar{p}_2^2 y_2^2}\int_{y_{20}}^{y_2} 4\beta_0^2\bar{p}_2^2 e^{-2\beta_0^2\bar{p}_2^2 u^2} u g(u) du.$$

Next, we rescale by $v = \sqrt{2}\beta_0\bar{p}_2 y_2$, $w = \sqrt{2}\beta_0\bar{p}_2 u$ to arrive at

$$\begin{aligned} h(v) &= h_0 e^{(v^2-v_0^2)} - 2e^{v^2}\int_{v_0}^{v} e^{-w^2} w g(\frac{w}{\sqrt{2}\beta_0\bar{p}_2})\, dw \\ &= h_0 e^{(v^2-v_0^2)} - 2e^{v^2}\int_{v_0}^{v} e^{-w^2}[Aw^2 + Bw^3 + Cw^4]\, dw \end{aligned}$$

where

$$A = \frac{\beta_1\,\bar{p}_1 - \beta_0\,p_0\,\cos(\theta)}{\sqrt{2}\,\beta_0\,\bar{p}_2},\ B = \frac{\beta_1\,\bar{p}_2 - \beta_0\,\bar{p}_1\,\cos(\theta)}{2\beta_0^2\,\bar{p}_2^2},\ C = -\frac{\cos(\theta)}{2\sqrt{2}\,\beta_0^2\,\bar{p}_2^2}.$$

Assume that $v_0 < 0$ and define $\delta = -\frac{1}{v_0}$ and $v = \frac{z}{\delta}$. When $\delta << 1$, i.e. $|v_0| >> 1$, we can derive the following asymptotic expression for $h(v)$, now in terms of z:

$$h(z) \approx (h_0 - B)e^{\delta^{-2}(z^2-1)} - (A + \frac{3}{2}\,C)\,\sqrt{\pi}\,e^{\delta^{-2}z^2}.$$

In terms of the original parameters, this can be written

$$h(z) \approx (h_0 - B)e^{\delta^{-2}(z^2-1)} + (M_2 - M_1\beta_1)\,\sqrt{\pi}\,e^{\delta^{-2}z^2}, \tag{22}$$

where

$$M_1 = \frac{\bar{p}_1}{\sqrt{2}\,\beta_0\,\bar{p}_2},\ M_2 = \frac{p_0\cos(\theta)}{\sqrt{2}\,\bar{p}_2} + \frac{3}{4\sqrt{2}}\frac{\cos(\theta)}{\beta_0^2\,\bar{p}_2^2}.$$

For the second term in (22) to remain bounded, we require

$$(M_2 - M_1\beta_1)\,\sqrt{\pi} = \mu e^{-\delta^{-2}k^2}. \tag{23}$$

for some positive $O(1)$ constant k, where $\mu = \pm 1$ is determined by the sign of $M_2 - M_1\beta_1$. This gives

$$h(z) = (h_0 - B)e^{\delta^{-2}(z^2-1)} + \mu e^{\delta^{-2}(z^2-k^2)}.$$

The analysis after this point again is similar to that in [15], and we refer the reader there for more details. The expression for $h(z)$ will be dominated by the second term if $|v_0|$ is sufficiently large. It follows that the trajectory of the perturbed system will lie outside (inside) the separatrix of the unperturbed system if $\mu = 1$ (-1). Since $M_1 > 0$ (in both the traditional and axial-torsional cases), $\mu = \pm 1$ if

$$\beta_1 \lessgtr \frac{M_2}{M_1} = \beta_c,$$

where β_c is defined by eq. (20).

So the trajectory ultimately lies inside the separatrix (and is attracted to the limit cycles born from the Hopf bifurcation) if $\beta_1 < \beta_c$. If $\beta_1 > \beta_c$ it lies outside the separatrix and is attracted to the relaxation limit cycles. So the switch from

small amplitude limit cycles to large amplitude limit cycles occurs at

$$\beta_1 = \beta_c = \left[\frac{\beta_0\, p_0}{\bar{p}_1} + \frac{3}{4}\frac{1}{\beta_0\, \bar{p}_1\, \bar{p}_2}\right] \cos(\theta) = \beta_H + \Delta\beta.$$

This is the critical value of β_1 where the amplitude of the limit cycle produced by the Hopf bifurcation grows without bound. Thus it marks the point where the canard transition to relaxation oscillations takes place, and coincides with the value computed in the previous section from the limit of the periodic solution criterion as the separatrix is approached. For instance, for the parameter values $p_0 = 0.8, \bar{p}_1 = 0.2, \bar{p}_2 = 0.1, \theta = 0$, we have $\beta_0 = 10$ and the switch point becomes $\beta_c = 43.75$. This is confirmed by the calculation of the bifurcation diagram shown in figure 4, where it is the value of β_1 where the amplitude of the cycle increases very rapidly.

5. Numerical Investigations

In order to investigate the range of validity of our various approximations we turn now to computational techniques. In particular, we simulate the DDE model (3) and its inertial manifold ODE (8) and use branch following methods to trace bifurcation curves.

Numerical simulations were carried out with MATLAB's ode45 for the ordinary differential equation approximation to the DDE, and MATLAB's dde23. Relative error tolerances ranged from the default 10^{-3}, to as little as 10^{-7}, for runs with parameter values near the transition to the canard cycle.

Numerical continuation of periodic solutions of the delay differential equation was performed using the package DDEBIFTOOL [18]. For the inertial manifold ordinary differential equation approximation to the DDE, the AUTO package contained in the program XPPAUT [19] was used. Both packages use collocation methods to approximate the periodic orbits and can thus approximate both stable and unstable solutions. For both packages we used 400 mesh intervals and degree 4 polynomials for approximation of the periodic orbits.

Numerical computation of canards is not easy, due to the sensitivity of the system to round-off error in both the phase space and parameter space. We refer the reader to [20] for a treatment of these issues. Collocation methods employed by the branch following routines perform better, but the results must be carefully examined near the transition from the small to the large orbit. We are confident of the validity of the bifurcation curves showing amplitude of solution versus β because these remain unchanged as we increase the accuracy of the computations. However, we do not trust the computations by AUTO and DDEBIFTOOL of the Floquet multipliers for the canard periodic orbits for the following reasons. The method used by both programs to compute Floquet multipliers is known to be inaccurate when the system has Floquet multipliers which are very large or close to zero [21] and we observed that the computed values were indeed very large on some parts of the computed branches. Further, Krupa and Szmolyan [22] have shown analytically that the nontrivial Floquet multiplier of a canard periodic orbit in a class of two dimensional ODE systems similar to (8) is either close to zero or very large.

To begin we compare the Hopf bifurcation β values for varying τ for the DDE model (3), the inertial manifold ODE (8), and the first order perturbation approximation to bifurcation value. In Figure 5 the β vs. τ curves are plotted that mark the Hopf bifurcation. The solid line denotes the boundary for the inertial manifold ODE (8) ($\beta_H vs. \tau$), the dashed line the linear approximation to β_H and the dotted

line is the analytic expression for the Hopf stability boundary for the DDE model (3). The bifurcation curve for the inertial manifold ODE lies above the linear approximation, with the difference growing larger with larger τ. We expect the linear approximation to the boundary to be valid only in the small τ limit, since the true boundary is a curve. The inertial manifold ODE captures the stability boundary for the DDE model up to the value where the DDE boundary turns downward, at which point the ODE cannot capture the more complex behaviour of the DDE. For both, the bifurcation has been shown to be supercritical.

In Figure 6 the transition from limit cycle to canard-type cycle to relaxation oscillation for (13) with $\tau = 0.1$ is demonstrated in the phase plane. We also plot the $y' = 0$ nullcline for (13) with β set to the Hopf bifurcation value, for illustration purposes. We note that these numerical simulations are sensitive to round-off error, especially for smaller values of τ. This can create a "banding" effect in the orbit, making it appear to be thickened, and/or cause it to cycle around both the large and small orbit. The vanishingly small region of parameter space over which the transition occurs also makes it difficult to find a sequence of orbits that smoothly transitions from small to large amplitude.

In Figure 7 we plot the curves marking the transition to the large canard cycle in the β vs. τ plane for all three cases. Note that the β value is not determined exactly, but is representative of a vanishingly small range of β over which the transition occurs. We compare the perturbation approximation to the canard transition line, $\beta = \beta_0 + \tau\beta_{1c}$ (where β_{1c} is determined by (20)), with a curve generated from numerically solving the inertial manifold ODE (8). Again this value lies above the linear approximation, and is concave up over the range examined, so that the difference grows with increasing τ (as would be expected from an asymptotic approximation in τ). The transition curve for the DDE model (3) was also estimated numerically. Somewhat surprisingly, the ODE and DDE behavior are still quantitatively quite close, even though the size of the orbit in the phase plane is growing large. The range in τ is smaller in this figure than in Figure 5, due to the difficulty in resolving a single clean transition value for the DDE. For τ larger than about 0.1 there is a more complicated transition to the large orbit in the DDE model, a matter we take up in the Discussion.

To further investigate the Hopf bifurcation and the growth of the large orbit in both the DDE model and its inertial manifold ODE approximation, branch following routines were employed (XPPAUT and DDEBIFTOOL respectively). We present in Figure 8 a) a numerical continuation of the Hopf bifurcation curve for the inertial manifold ODE (8) with $\tau = 0.05$. In part b) of that figure periodic orbits corresponding to increasing β values are shown. These orbits, computed via collocation, give a more complete representation of the canard transition than can be found by numerical simulation of the ODE, due to the vanishingly small range of β over which it occurs. The orbit starts small, grows to an amplitude where it reaches the knee of the critical manifold, at which point the orbit turns up instead of down before it completes the cycle. At larger τ values it leaves the vicinity of the critical manifold for smaller and smaller y values, until it becomes the large cycle. This occurs over a very small range of β, as indicated by the almost vertical transition in the numerical bifurcation diagram. AUTO indicates the that the branch of periodic orbits is stable, except for a section of the vertical part of the branch. As indicated above, the computation of Floquet multipliers along this part of the branch cannot be trusted. Other studies of canard explosions in ODE systems similar to (8) have shown numerically [15] and analytically [22] that if the canard explosion originates in a supercritical Hopf bifurcation then the entire branch of periodic orbits is stable. We believe the same is true for the inertial

manifold ODE (8).

A similar diagram following the branch of periodic solutions from the Hopf bifurcation for the DDE model is shown in figure 9 a). This was created with the branch following routine in DDEBIFTOOL [18]. The bifurcation parameter in the graph is β, and the delay is fixed at $\tau = 0.05$. The other parameters are as in the previous section. We note that shortly after the Hopf bifurcation at $\beta = 12.5$, the rapid transition to large amplitude cycles is seen ($\beta \approx 12.75$). In figure 9 b) representative orbits from the transition are plotted. These were determined by collocation and the canard cycle is found in the progression from small to large periodic orbits. DDEBIFTOOL indicates the that the branch of periodic orbits is stable, except for a section of the vertical part of the branch. As indicated above, the computation of Floquet mulipliers along this part of the branch cannot be trusted. Numerical simulations of the DDE (3) (see Fig. 6) seem to indicate stability everywhere along the branch.

We close this section by reporting that the approximation to this order fails when τ grows larger than about 0.1. A complicated transition to the large orbit involving period doubling is observed, see figure 10 a), which was also computed using DDEBIFTOOL for $\tau = 0.2$. Example of orbits from this sequence are shown in figure 10 b). This behaviour will be the subject of future investigations.

6. Discussion

Although we have focussed on a particular DDE due to our interest in the physical system it models, the canard transition we observe should occur in other systems with time delays. The basic ingredient is simple: for zero delay the system has a "degenerate" Hopf bifurcation, i.e., at a particular value of the bifurcation parameter the system is conservative and has an equilibrium point which is a nonlinear centre. Baer and Erneux [15, 16] showed that perturbing an ODE with such point can lead to the canard transition. We have extended this to show that the perturbation may be the introduction of a time delay. We expect that one could "design" a system with a canard transition by the appropriate introduction of a time delay into an ODE with a nonlinear centre.

Specifically, for our machining model in the high speed limit, $\tau \to 0$, we found a center manifold approximation to the delay differential equation that is conservative if the viscous damping term is removed. This ODE can be solved exactly, and solutions to it form the backbone of the analysis for small τ. In particular, the separatrix between unbounded and bounded solutions found in the singular limit (both delay and damping vanish) determines the form of the oscillation for small delay and damping.

The small τ approximation to the DDE possesses a supercritical Hopf bifurcation for the drilling model parameters, and perturbations of the Hopf bifurcation parameter β for fixed τ allow us to compute the behavior of the branch of limit cycle solutions that emerge at β_H. We see that this branch diverges at a critical β value (β_c) where the small periodic orbit jumps to the large cycle in a canard explosion. Following the analysis in [15] we find solutions close to the separatrix from the conservative system to show the large cycle exists and arises smoothly from the small orbit as the bifurcation parameter is increased.

In the last section we used numerical methods to evaluate the validity of the asymptotic approximation to solutions found in section 4. Numerical simulation of both the ODE and the DDE demonstrated the Hopf bifurcation and the transition to the large orbit. Numerical branch following/continuation methods were used to construct bifurcation diagrams for the period orbits. We also used these programs

to compute limit cycle solutions along the branch via collocation methods. The smaller the value of τ used, the more singular the transition to the large orbit becomes. This is typical of canard type transitions, which are notoriously difficult to find as the region of parameter space in which they occur becomes exponentially small. We also observed the numerical instability demonstrated in [20], where orbits close to the transition are sensitive to round-off error and can switch erratically between large and small orbits.

While the high speed limit is not physical, and would not be attainable in real life machining processes, the solutions obtained using it shed light on the behaviour for more realistic values of the delay. In particular, the existence of a rapid transition to large amplitude oscillations from small orbits, is important to identify. This jump to large orbit is a concern, since it implies a dramatic loss of stability in the process. A similar sort of transition can be found in systems with a subcritical Hopf, where a small unstable limit cycle keeps solutions bounded near the steady cutting state, so long as they are initiated inside that orbit. Here, even though the initial Hopf bifurcation is supercritical, the behaviour is reminiscent of a subcritical Hopf, except that the perturbations responsible are in the bifurcation parameter rather than in phase space.

Finally, we note that increasing τ away from the singular limit results in some very complicated dynamics (period doubling and mixed mode oscillations) that we will take up in a future paper.

Acknowledgments

E.S. and S.A.C. would like to thank the University of Montana-Missoula PArtnership for Comprehensive Equity (PACE) for travel support. S.A.C. also acknowledges the support of NSERC. The research of T.E. was supported by the Fonds National de la Recherche Scientifique (Belgium).

References

[1] E. Stone and A. Askari, *Nonlinear models of chatter in drilling processes*, Dynamical Systems 17 (2002), pp. 65–85.
[2] C. Chicone, *Inertial and slow manifolds for delay differential equations*, J. Diff. Eqs. 190 (2003), pp. 364–406.
[3] J. Callot, F. Diener, and M. Diener, *Le problème de la chasse au canard*, C.R. Acad. Sc. Paris Série A 286 (1978), pp. 1059–1961.
[4] E. Benoît, J. Callot, F. Diener, and M. Diener, *Chasse au canard*, Collectanea Mathematica 31 (1981), pp. 37–119.
[5] W. Eckhaus, *Relaxation oscillations including a standard chase on French ducks*, Asymptotic Analysis II, Springer Lecture Notes Math 985 (1983), pp. 449–494.
[6] E. Schöll and H. Schuster *Handbook of Chaos Control 2nd Rev. Enl. Edition*, Wiley-VCH, Weinheim, 2007.
[7] T. Erneux, L. Larger, M. Lee, and J. Goedgebuer, *Ikeda Hopf bifurcation revisited*, Physica D 194 (2004), pp. 49–64.
[8] T. Erneux *Applied Delay Differential Equations*, ??, New York, 2008.
[9] M. Merchant, *Mechanics of the cutting process*, J. Appl. Phys. 16 (1945), p. 267.
[10] P. Oxley *The mechanics of machining*, Ellis Horwood Ltd., Chincester, 1989.
[11] E. Stone and S. Campbell, *Stability and bifurcation analysis of a nonlinear DDE model for drilling*, Journal of Nonlinear Science 14 (2004), pp. 27–57.
[12] J. Bélair and S.A. Campbell, *Stability and bifurcations of equilibria in a multiple-delayed differential equation*, SIAM J. Appl. Math. 54 (1994), pp. 1402–1424.
[13] T. Faria and L. Magalhães, *Normal Forms for Retarded Functional Differential Equations with Parameters and Applications to Hopf Bifurcation*, J. Diff. Eqs. 122 (1995), pp. 181–200.
[14] W. Wischert, A. Wunderlin, A. Pelster, M. Olivier, and J. Groslambert, *Delay-induced instabilities in nonlinear feedback systems*, Phys. Rev. E 49 (1994), pp. 203–219.
[15] S. Baer and T. Erneux, *Singular Hopf bifurcation to relaxation oscillations*, SIAM J. Appl. Math. 46 (1986), pp. 721–739.
[16] ———, *Singular Hopf bifurcation to relaxation oscillations II*, SIAM J. Appl. Math. 52 (1992), pp. 1651–1664.

[17] J. Guckenheimer and P. Holmes *Nonlinear Oscillations, Dynamical Systems and Bifurcations of Vector Fields*, Springer-Verlag, New York, 1983.
[18] G.S. K. Engelborghs T.Luzyanina, *DDE-BIFTOOL v. 2.00: a Matlab package for bifurcation analysis of delay differential equations.*, TW-330, Department of Computer Science, K.U. Leuven, Leuven, Belgium, 2001.
[19] G. Ermentrout *Similating, Analyzing and Animating Dynamical Systems: A Guide to XPPAUT for Researcher and Students.*, SIAM, Philadelphia, PA, 2002.
[20] J. Guckenheimer, K. Hoffman, and W. Weckesser, *Numerical computation of canards*, Int. J. Bifurc. Chaos 10 (2000), pp. 2669–2687.
[21] K. Lust, *Improved Numerical Floquet Multipliers*, 11 (2001), pp. 2389–2410.
[22] M. Krupa and P. Szmolyan, *Relaxation Oscillation and Canard Explosion*, J. Diff. Eqs. 174 (2001), pp. 312–368.

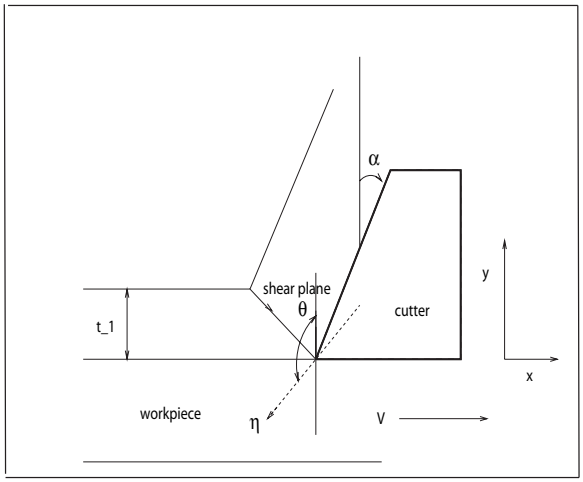

Figure 1. Diagram of cutting tool and workpiece in an orthogonal cutting operation. t_1 is the chip thickness, V is the cutting speed, α is the rake angle of the tool, θ is the vibration angle, and η is the vibration amplitude.

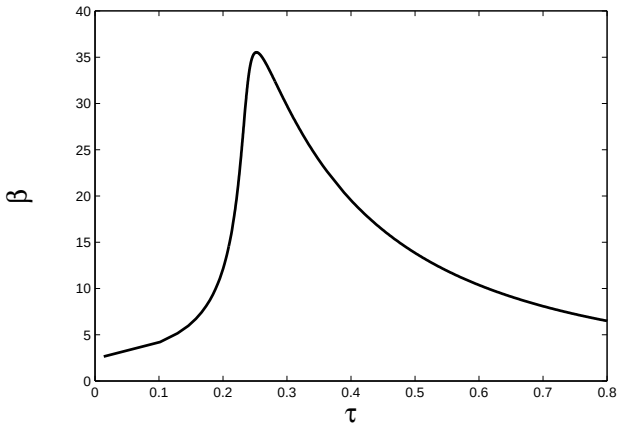

Figure 2. Hopf bifurcation boundary for the machining model for small values of τ ($n = 0$ branch) and $p_0 = 0.8$, $\bar{p}_1 = 0.2$, $\gamma = 0.5$, $\theta = 0$. See equation (4).

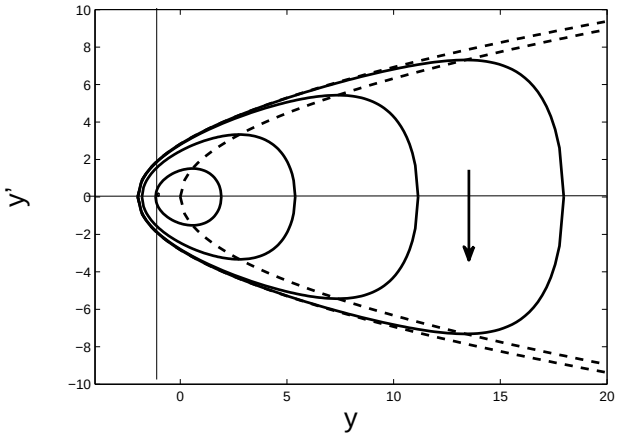

Figure 3. Closed orbit solutions to the conservative system (6). The values of the parameters are $\gamma = 0.5$, $\bar{p}_1 = 0.2$, $\bar{p}_2 = 0.1$, and $\beta = \beta_0 = \gamma/\bar{p}_1 = 2.5$. The outer dashed curve is the separatrix, given by (7), which separates the closed orbit solutions from the unbounded ones. The inner dashed curve is the $y' = 0$ nullcline.

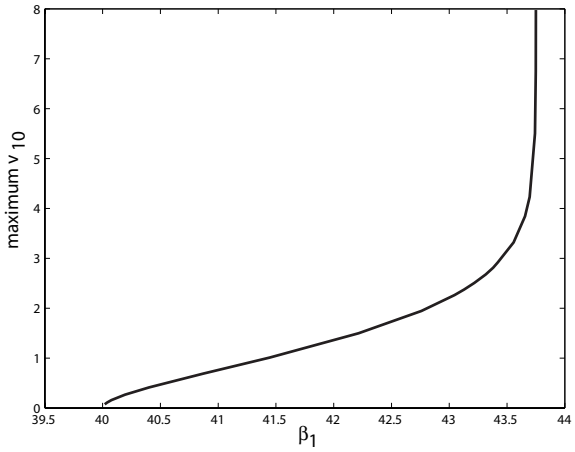

Figure 4. Bifurcation diagram for the amplitude of periodic solutions as $\tau \to 0$ (i.e. for the small τ limit of the inertial manifold ODE (13), computing by using equation (19). The x-axis is the bifurcation parameter β_1, and the y-axis is the first component of the expansion for the position variable v_1 in system (15). The values of the parameters are $\beta_0 = 10$, $p_0 = 0.8$, $\bar{p}_1 = 0.2$, $\bar{p}_2 = 0.1$. The Hopf bifurcation is located at $\beta_1 = 40$ and the amplitude becomes unbounded at $\beta_1 = \beta_c = 43.75$, marking the transition to the large amplitude cycle.

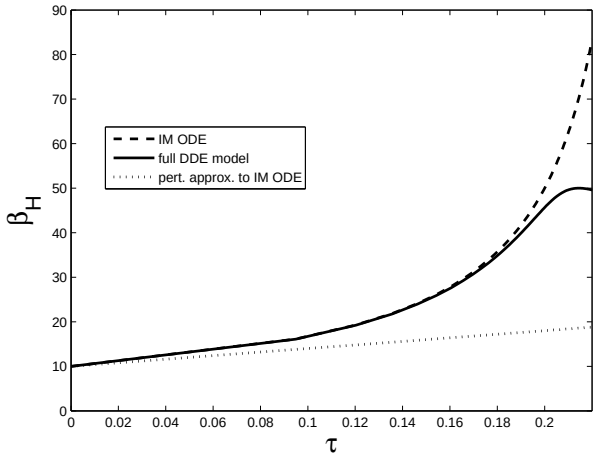

Figure 5. Comparison of Hopf bifurcation curves for the two systems for varying τ. The values of the parameters are $p_0 = 0.8$, $\bar{p}_1 = 0.2$, $\bar{p}_2 = 0.1$. The Hopf bifurcation curve for the inertial manifold ODE (8) is denoted by the dark hatched line and is given by $\beta = \frac{\gamma}{\bar{p}_1 - \tau p_0 \cos(\theta)}$. In the limit of small τ, this reduces to a bifurcation line (light hatched) which is given by $\beta_H = \beta_0 + \tau \beta_{1H}$, where $\beta_0 = \frac{\gamma}{\bar{p}1} = 10.0$ and $\beta_{1H} = \frac{\gamma p_0 \cos(\theta)}{\bar{p}_1^2} = 40.0$ for these parameter values. The bifurcation curve for the DDE model (3)is found from the Hopf bifurcation conditions for a purely imaginary eigenvalue (4) and is denoted by the solid line.

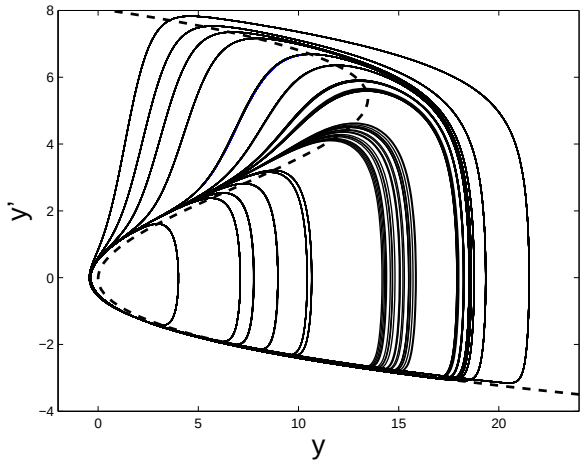

Figure 6. Phase plane of the solution to (8) for varying values of β. The transition to the canard cycle is shown, to be compared with the $y' = 0$ isocline for the system at the Hopf bifurcation value of β. The values of the parameters are $p_0 = 0.8$, $\bar{p}_1 = 0.2$, $\bar{p}_2 = 0.1$, $\tau = 0.1$, β ranging from 17.25 to 20.0.

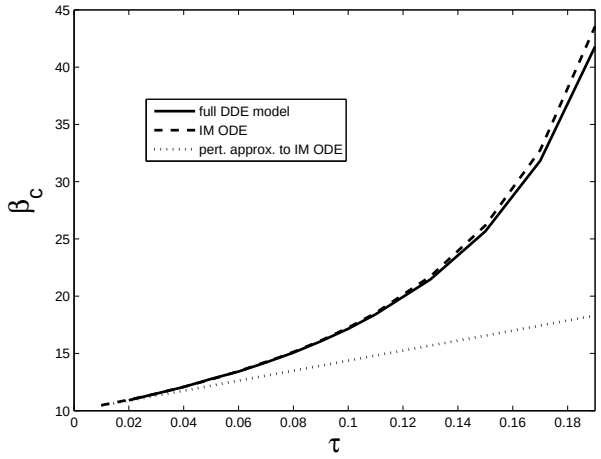

Figure 7. Comparison of transition curves from small to large limit cycles for the inertial manifold ODE and the DDE model for varying τ. The values of the parameters are $p_0 = 0.8$, $\bar{p}_1 = 0.2$, $\bar{p}_2 = 0.1$. The linear approximation to the transition for the inertial manifold ODE (8) is given by $\beta_c = \beta_0 + \tau\beta_{1c}$, where $\beta_0 = 10.0$ and $\beta_{1c} = 43.75$. The transition curve for the inertial manifold ODE (8) (dashed line) and the DDE model (3) (solid line) were computed numerically.

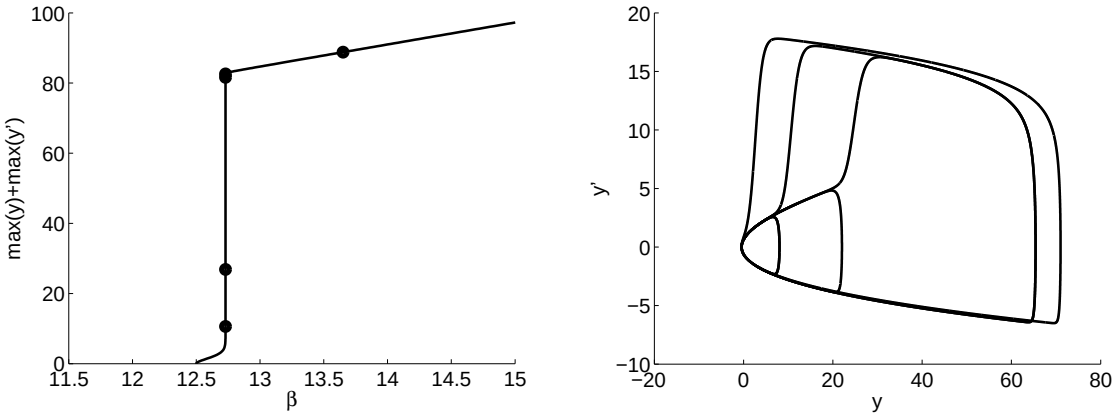

(a) (b)

Figure 8. (a) Numerical bifurcation diagram for the inertial manifold ODE (8) with $\tau = 0.05$, showing canard transition at $\beta \approx 12.73$. The value predicted by the perturbation theory analysis is $\beta = 12.1875$. The points marked with a • correspond to the periodic solutions shown in (b).

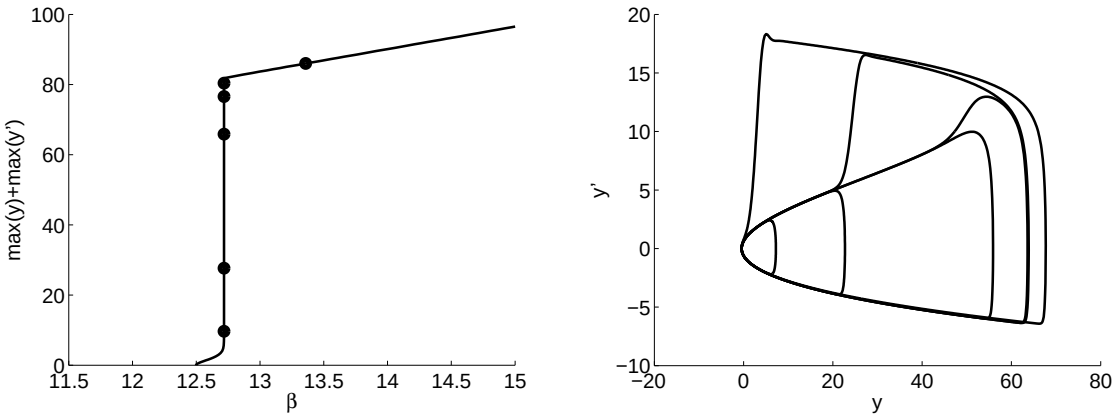

(a) (b)

Figure 9. (a) Numerical bifurcation diagram for full DDE model (3) with $\tau = 0.05$, showing canard transition at $\beta \approx 12.75$. The points marked with a • correspond to the periodic solutions shown in (b).

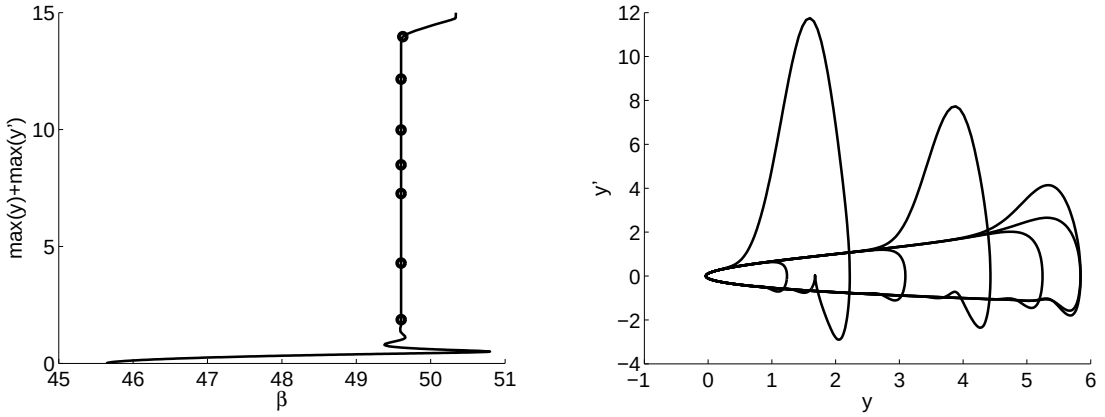

(a) (b)

Figure 10. (a) Numerical bifurcation diagram for full DDE model (3) with $\tau = 0.2$, showing a complicated transition to the large orbit at $\beta_1 \approx 49.5$. The points marked with a • correspond to the periodic solutions shown in (b).